Bioorganic Chemistry 88 (2019) 102953

Contents lists available at ScienceDirect

Bioorganic Chemistry

journal homepage: www.elsevier.com/locate/bioorg

Discovery of Baicalin as NDM-1 inhibitor: Virtual screening, biological evaluation and molecular simulation

Cheng Shi, Jingxiao Bao, Ying Sun, Xinyue Kang, Xingzhen Lao*, Heng Zheng*

School of Life Science and Technology, China Pharmaceutical University, Nanjing 210009, PR China

ARTICLE INFO

Keywords:
NDM-1 inhibitors
Natural products
Virtual screening
Molecular dynamics simulation

ABSTRACT

The emergence and worldwide spreads of carbapenemase producing bacteria, especially New Delhi metallo-β-lactamase (NDM-1), has made a great challenge to treat antibiotics-resistant bacterial infections. It can hydrolyse almost all β-lactam antibacterials. Unfortunately, there are no clinically useful inhibitors of NDM-1. In this study, structure-based virtual screening method led to the identification of Baicalin as a novel NDM-1 inhibitor. Inhibitory assays showed that Baicalin possessed a good inhibition of NDM-1 with IC_{50} values of 3.89 ± 1.1 μM and restored the susceptibility of *E.coli* BL21(DE3)/pET28a-NDM-1 to clinically used β-lactam antibiotics. Molecular docking and molecular dynamics simulations obtained a complex structure between the relatively stable inhibitor molecule Baicalin and NDM-1 enzyme. The results showed that the carboxyl group in Baicalin directly interacted with the Zn^{2+} in the active center of the enzyme, and the residues such as Glu152, Gln123, Met67, Trp93 and Phe70 in the enzyme formed hydrogen bonds with Baicalin to further stabilize the complex structure.

1. Introduction

β-lactams(penicillins, carbapenems, cephalosporins and monocyclic lactams) have been one of the most important and commonly used classes of antibiotics in medicine due to their broad spectrum, high efficiency and low toxicity [1]. However, with the widespread use and even abuse of β-lactam drugs, the main pathogens have produced various resistance mechanisms to β-lactams, and the most important is the catalytic hydrolysis by metallo-β-lactamases (MBLs). These enzymes can activate nucleophilic water to cut invariant β-lactam bond and confer resistance to bacteria [2]. At present, the speed of identifying new antibiotics has been greatly slowed down in recent decades [3]. It has been dedicated to discover the use of MBLs inhibitors in combination with existing β-lactams to restore the efficacy of β-lactams against MBLs-producing bacteria. This strategy has been successfully applied to serine-β-lactamases (SBLs) clinically, and can act as a catalytic nucleophile against the SBLs through the active site Ser residue [4].

MBLs are a class of β-lactamases, which pose a serious threat to human health. There are three subclasses in MBLs, B1, B2 and B3, and clinically relevant inhibitors for the MBLs are currently not available [5], New Delhi metallo-beta-lactamases (NDM-1) was firstly reported on 2009, which belongs to the class B MBLs superfamily [6]. NDM-1 mediated drug resistance has received great attention because it can hydrolyze almost all kind of beta-lactam antibiotics except monobactams [7]. In addition, the high transferability of NDM-1 related resistance also causes great panic. This resistance has been identified in many popular human pathogens, including *Enterobacteriaceae*, *Pseudomonas* and *Acinetobacter*, and is often accompanied by genes encoding other resistance determinants [8,9]. Currently, few effective treatment regimens are available to combat this so-called “superbug” infection.

Natural products have played a critical role in the history of drug discovery [10,11]. These compounds generally have weaker antibacterial activity, but recent studies have shown that a variety of natural products have the effect of restoring bacteria's susceptibility to antibiotics, and even reverse the resistance of bacteria to certain antibiotics, Therefore, the combination of antibiotics and natural products provides new ideas for the treatment of resistant bacteria infections [12–15]. In the present study, we successfully identified a potent NDM-1 inhibitor, namely Baicalin, through virtual screening of a natural product library. Baicalin is the main bioactive compound derived from traditional Chinese medicine radix of *Scutellaria baicalensis*. To our knowledge, it is the first report that Baicalin possesses direct inhibit effects on metallo-β-lactamase, although the herb *Scutellaria baicalensis* has been used as traditional Chinese medicine about two thousands of years ago. We verified its inhibition by monitoring the substrate changes using high performance liquid chromatography (HPLC). Considering the flexibility of the active site of MBLs, we also obtained the

* Corresponding authors.
E-mail addresses: lao@cpu.edu.cn (X. Lao), zhengh18@hotmail.com (H. Zheng).

https://doi.org/10.1016/j.bioorg.2019.102953
Received 10 February 2019; Received in revised form 15 April 2019; Accepted 24 April 2019
Available online 27 April 2019

optimal stable structure of the complex Baicalin-NDM-1 by molecular dynamics simulation of the docking results. The complex structure not only lays a foundation for studying the inhibitory mechanism of inhibitors on NDM-1, but also helps for the design of more reasonable inhibitors.

2. Methods and materials

2.1. Structure-based virtual screening

The virtual screening was performed with MOE2016 implemented within MOE's Dock. The Dock application looks for a favorable binding pattern between the ligand and the target. For each ligand, a number of placements called poses are generated and scored, including contributions, solvation and entropy terms, or based on Polar interaction energy (including metal connections) or numerical values based on qualitative shapes [16]. To identify new MBLs inhibitors, a natural product library was virtually screened starting with the available NDM-1 crystal structure. Specifically, NDM-1 and ampicillin structures were separately extracted from the complex structure of NDM-1 hydrolyzed ampicillin (PDB:5ZGE) and pretreated (hydrogenation, charge, structure correction, etc.). Using the NDM-1 and ampicillin structures extracted in the previous step, multiple docking procedures with different parameters were performed. By comparing the level of the GBVI/WSA dG score of the docking result and the difference from the original composite structure, the docking parameters are determined and the screening model is established. The GBVI/WSA dG is a forcefield-based scoring function which estimates the free energy of binding of the ligand from a given pose. The calculation formula is as follows [17]:

$$\Delta G \approx c + \alpha\left[\frac{2}{3}(\Delta E_{coul} + \Delta E_{sol}) + \Delta E_{vdw} + \beta \Delta SA_{weighted}\right]$$

where

c represents the average gain/loss of rotational and translational entropy. α,β are constants which were determined during training (along with c) and are forcefield-dependent. If not using an AMBER forcefield, the parameters will be set by default to the MMFF trained parameters. E_{coul} is the coulombic electrostatic term which is calculated using currently loaded charges, using a constant dielectric of 1. E_{sol} is the solvation electrostatic term which is calculated using the GB/VI solvation model. E_{vdw} is the van der Waals contribution to binding. $SA_{weighted}$ is the surface area, weighted by exposure. This weighting scheme penalizes exposed surface area.

Pre-treating the structure of natural products in library, including eliminating possible system structural errors in the database (alkali metal-oxygen single bonds, protonated strong acids, deprotonated strong bases), calculating and setting partial charges for all molecules in the database and Minimize structure, etc.

NDM-1 was used as a receptor to sequentially dock small molecule ligands in the natural compound pool. Screening for small molecule ligands with high binding activity according to the parameters determined in the above steps.

2.2. Construction of NDM-1 strain and expression purification

The wild type NDM-1 gene lacking the signal peptide was synthesized and then cloned between EcoRI and Hind III restriction sites into the pET-28a plasmid harboring a kanamycin resistance gene [18]. The constructed plasmid encoding NDM-1 was transferred into *E. coli* BL21(DE3). NDM-1 enzyme was expressed and purified as shen described [19].

2.3. Determination of the IC_{50} values

NDM-1 (final concentration 10 nM) supplemented with 50 mM HEPES buffer containing 100 μM Zn^{2+} was first pre-incubated on a dry bath at 30 °C for 5 min to allow Zn^{2+} to fully occupy its active site. The enzyme was then incubated for an additional 5 min with different concentrations of inhibitor. and transferred to a quartz cuvette. Cefuroxime sodium (final concentration 60 μM) was added, mixed immediately and the initial rate of substrate hydrolysis was recorded at 260 nm using UV-1800 spectrophotometer. All experiments were repeated three times. The inhibition rate was calculated by the following equation and the IC_{50} value was calculated by plotting the regression equation of the inhibitor concentration against the percentage of the mean inhibition rate [20].

$$I = \left(1 - \frac{V_i}{V_0}\right) \times 100\%$$

where

V_0 is the initial rate of reaction without inhibitor and V_i is the initial rate of reaction at different inhibitor concentrations.

2.4. Measurement of inhibitory effect by HPLC-based method

The enzyme reaction were prepared as IC_{50} determination method discribed in 2.3. The reaction were stoped by adding 2 μl of metal chelator EDTA (5 mM) after 5 min incubation. The inhibitory activity of the inhibitors was calculated as: $Ir = 1 - (A_i - A_x)/(A_i - A_0) \times 100\%$, where *Ir* was inhibitory rate, A_0 was the peak area after the reaction in the absence of inhibitors, and A_i, A_x represented the peak area before and after the reaction in the presence of the screened inhibitors in different concentrations. The Agilent 1100 Series LC system (Agilent, USA) controlled by the Agilent Chem Station Software and fitted with an Alltech Apollo 5u C18 column (250 mm × 4.6 mm ID) was used to detect the concentrations of phenol and metabolites. The operating conditions were as follows: room temperature; mobile phase, deionized water/acetonitrile (70:30, v/v) with a solvent flow rate of 1.0 mL/min. The detailed parameters are set as follows: A solvent: B solvent = 85 (Sodium acetate, pH 3.4): 15 (Acetonitrile); and flow is 1.2 mL/min and absorption wavelength 260 nm.

2.5. Minimum inhibitory concentration (MIC) and fractional inhibitory concentration index (FICI) determination

MICs for *E.coli* BL21 (DE3) harboring NDM-1 were determined by a two-fold checkerboard microdilution on 96-well microplatesas as previously described. [21] *E.coli* BL21 (DE3)/pET-28a was used as negative control. The concentrations of inhibitors were varied between 1 μg/mL and 64 μg/mL in serial ½ dilutions, and the bacteria was diluted to 1×10^6 CFU/mL by Luria-Bertani (LB) broth containing 50 μg/mL kanamycin and 0.2 mM IPTG. All wells were complemented with the LB medium to give a final volume of 100 μl and then incubated at 37 °C for 12 h. A reading at 595 nm was taken to determine the MICs. All experiments were performed in triplicate. Then, to verify the ability of the compound to synergically interact with therapeutically available antibiotics, the FICI for each compound was calculated as the lowest concentration in the presence of co-compound for a well showing no growth, divided by the MIC for that compound alone. The FICI is the sum of the two FICIs. Synergy was defined when FIC index ≤ 0.5, while antagonism was defined when FICI > 4. A FICI between 0.5 and 4 (0.5 < FICI ≤ 4) was considered indifferent [22].

2.6. Molecular dynamics simulation

2.6.1. Model processing

In the simulation process, for the ligand molecule, the GAFF force field in Amber was used. The atomic charge was optimized by the HF method in the 6-31G* basis group and then the RESP charge was fitted using the antechamber program in AmberTools. The treatment of NDM-1 is as follows: zinc ions are treated with a cationic virtual atom model,

and the His-coordinated is processed into a HIN form according to the requirements of the model (ie, both protons are on both nitrogen atoms in the His side chain) [23]. Cys is treated as a CYM form (ie, the sulfur atom in the Cys side chain is deprotonated), and Asp is treated to a normal ASP form (ie, the oxygen atom on the carboxyl group of the side chain is deprotonated). Since the first two residues of the *N*-terminus of the protein are deleted in the PDB structure, we add an ACE "hat" (ie, a $-C{=}O-CH_3$ group) at the *N*-terminus of the first Glu30 residue that records structural information. To neutralize the charge on the *N*-terminal amino group. The force field parameters of the ff14SB force field, zinc ion, HIN residue, and bridged hydroxyl group were obtained from Pang's report [24]. The TIP3P water molecular box using a truncated regular octahedron simulates the solvent environment [25]. Any atom in the protein is at least 10.0 Å from the edge of the water box. Na^+ ions are added as counter ions to maintain the system neutral. The ion parameters are derived from frcmod.ions1lsm_hfe_tip3p document [26].

2.6.2. Dynamics simulation

For the initial system, firstly, the 2500-step steepest descent method and the 2500-step conjugation are performed under the condition that a binding force of 5.00 kcal·mol^{-1}·Å^{-2} is applied to the protein atom (including the zinc ion and the hydroxyl group of the active site). Gradient energy optimization removes possible space collisions between solvent molecules and between solvent and protein molecules. Then, the unconstrained 5000-step steepest descent method and the 5000-step conjugate gradient method energy optimization are performed on the whole system to further remove the collision between atoms. In the energy optimization process, the interaction between all bonding atoms is calculated. The cutoff value of the long-range non-bond interaction is set to 10.0 Å. Using the periodic boundary of constant volume, the long-range electrostatic interaction is calculated using the PME (Particle Mesh Ewald) algorithm [27]. Function, other parameters use the default value.

The optimized system is then subjected to a temperature increase treatment. The system was slowly heated from 0 K to 300.0 K in 500 ps, applying a binding force of 2.00 kcal·mol^{-1}·Å^{-2} to proteins (including zinc ions and hydroxyl groups), using a collision frequency of 2.0 ps^{-1} and a thermal bath. The Langevin constant temperature algorithm with a coupling constant of 1.0 ps uses the SHAKE algorithm to constrain the bond length of a bond containing a hydrogen atom, the integration step size is set to 2.0 fs, and the long-range cutoff value is also set to 10.0 Å [28,29]. Use constant volume periodic boundaries and PME algorithms, and other parameters use default values.

The system pressure is then balanced. The equilibrium process is carried out in five rounds, each round of 1 ns. During the equilibrium process, the protein skeleton atoms and zinc ions and hydroxyl groups are bound, and the binding force is from 1.00 kcal·mol^{-1}·Å^{-2}, followed by 0.50, 0.25, 0.10, and finally to 0.05. Using the Monte Carlo constant pressure algorithm, the target pressure is set to 1.0 bar, the pressure relaxation time is set to 2.0 ps, the periodic boundary of constant pressure is used, and the Langevin constant temperature algorithm is used to maintain a constant temperature of 300.0 K [30]. Other parameters and temperature rise process consistent.

Finally, the system was subjected to a long-term dynamic simulation of 100 ns at a constant temperature of 300.0 K and a constant pressure of 1.0 bar, and the atomic coordinates of the system were recorded every 10 ps to obtain the kinetic trajectory.

3. Results and discussion

3.1. Screening results and inhibitory capabilities of the screened inhibitors

The top 1 percent of the compounds in the screening result were selected for molecular docking. According to the interaction between the compound and NDM-1 6 compounds were hit and purchased. The results of the inhibition of NDM-1 by these compounds are shown in Table 1. The compound 5 and 6 are failed to determine inhibitory capability due to the poor solubility.

Table 1
Structures and IC_{50} values on NDM-1 of the screened inhibitors.

Compounds	Name	Structure	IC_{50} (μM) [a]
1	Baicalin	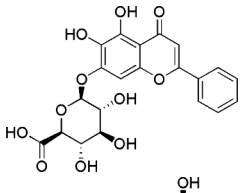	3.89 ± 1.1
2	Hyperoside	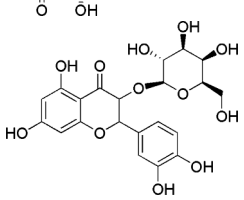	80 ± 3.5
3	Matrine	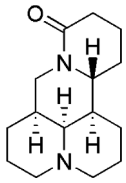	16 ± 0.8
4	Jaundice	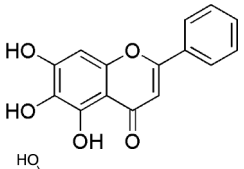	8.1 ± 1.2
5	–	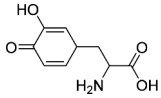	Not detected
6	–	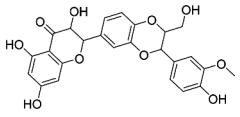	Not detected

3.2. High performance liquid chromatography (HPLC) analysis

Inhibition analysis showed that Baicalin had the best inhibitory effect on NDM-1 with IC_{50} of 3.89 ± 1.1 μM. In addition, compound 4, which is a Baicalin analogue, also has a good inhibitory effect. Therefore, the Baicalin is selected for further study. Traditional methods for detecting substrate changes using the UV spectrophotometer method may be affected by the potential absorption of the inhibitor or products. In addition, new substances that may be produced during the reaction will also affect the results. Here, we try to use high performance liquid chromatography (HPLC) to detect substrate changes to verify the inhibitory capacity of Baicalin. It can evaluate the inhibitory effect of inhibitors after a transient but constant process of enzymatic hydrolysis. The results are shown in Fig. 1, using HPLC to monitor the change of the substrate cefuroxime after a period of reaction. The method has the advantages that the inhibitor, the cephalosporin and the hydrolyzate can be separated, the interference of other interference factors on the experimental results is excluded, and the change of the hydrolyzate is more accurately supervised. The results of HPLC confirmed the inhibitory effect of Baicalin on NDM-1, and And when the inhibitor concentration reaches 8 μM, the inhibition rate to NDM-1 can reach 90%.

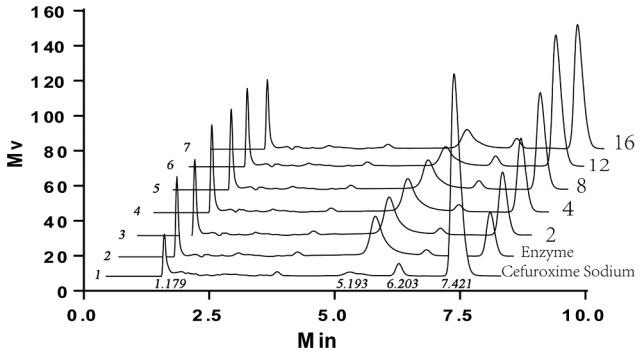

Fig. 1. HPLC results show the inhibition of hydrolysis ability of NDM-1 on Cefuroxime Sodium. The ordinate is expressed as the total response value (Mv) of various components in the system, and the abscissa represents time (Min). Curve 1 does not contain NDM-1 enzymes and inhibitors. Curve 2 contains the NDM-1 enzyme, and curves 3-7 contain the NDM-1 enzyme and different concentrations of inhibitors (2, 4, 8, 12, 16, 20 μM) The peak appearing at 1.179 minutes was EDTA (used to terminate the reaction with a final concentration of 5 mM). The peak appearing at 5.193 is the reaction product. 6.203 and the part between 1.179 and 5.193 may be the solvent peak. The peak appearing in 7.421 is cefuroxime sodium.

3.3. The MICs and FIC index

Monitor the hydrolytic decomposition of the carbapenem antibiotic inside *E.coli* cells expressing NDM-1are currently preferred choice to filter potential MBLs inhibitors [31]. In this experiment, *E.coli* BL21(DE3)/pET28a-NDM-1 presents high resistance with an MIC of 64 or 128 μg/mL for Cerfuroxime or Ampicillin, compared to *E.coli* BL21(DE3)/pET28a with an MIC of 0.5 and 1 μg/mL, respectively. Apparently, the presence of Baicalin who is able to inhibit NDM-1 activity successfully reduces the MIC for Ampcillin from 128 μg/mL to 8 μg/mL, and Cefuroxime Sodium from 64 to 4 μg/mL, respectively (Fig. 2). As a bioactive component in edible medicinal plants, Baicalin itself has moderate antibacterial activity with a MIC ≥ 512 μg/mL. When combined with the two antibiotics, the MICs for Baicalin varied between 32 μg/mL and 64 μg/mL. It has been reported that Baicalin can enhance LYSO-induced bacteriostasis during the innate immune response to S. aureus., and suggested to be a potentially useful therapeutic agent for the treatment of bacterial infections [32]. We conclude that Baicalin synergically interact with the two antibiotics by FIC index shown in Table 2.

Table 2
In vitro interaction between antibiotics and Baicalin (MIC unit: μg/mL).

Antibiotic	*E.coli* BL21(DE3) /pET28a	*E.coli* BL21(DE3) /pET28a-NDM-1	FICI
Ampcillin	1	128	
Ampcillin + Baicalin		8	≤0.19
Cefuroxime	0.5	64	
Cefuroxime + Baicalin		4	≤0.125
Baicalin		≥512	

3.4. Molecular dynamics simulations

3.4.1. Rationality analysis of docking results

Since the natural conformation of the complex should be the lowest energy stable binding conformation, we can evaluate the rationality of the interaction mode of the complex by calculating the binding stability of the inhibitor molecule to the enzyme. Molecular dynamics simulations (MD) were performed on the top 10 ranked docking poses (Fig. 3) using the Amber14 program [33]. First, two long-term (100 ns) kinetic simulations were performed on the 10 composite structures previously obtained. For the simulated trajectories, after stacking based on the overall structure of the composite, the stability of ligand binding is determined by calculating the mass-weighted root-mean-square deviation (RMSD) value of the heavy atoms in the ligand. The change in the ligand RMSD value (referenced to the structure at 50 ns) in the 20 kinetic trajectories of the 10 composite structures is shown in Fig. S1. The trajectory with relatively stable ligand molecule binding was screened for subsequent studies (actually a total of 9 were selected, M1_D1, M1_D2, M2_D1, M2_D2, M5_D2, M6_D2, M8_D1, M8_D2, M10_D1). Next, we performed a second round of dynamics simulation of the composite structure at the last moment of the nine trajectories (renamed M1 to M9 in turn). In addition to calculating the RMSD value of the heavy atom in the ligand (referenced to the initial structure) to reflect the binding stability of the ligand, the RMSD value of the acceptor heavy atom in the initial structure that is less than 10.0 Å from any atom in the ligand molecule was introduced to evaluate the change in the central structure of the acceptor (Fig. S2). The mass-weighted root-mean-square fluctuations (RMSF) values of the weight-bearing atoms were used to characterize the ligand stability (Fig. 4a). It can be seen that the RMSF values of the complexes M1, M2, M4, M5, and M8 are restively small, But in complexes M1, M5, and M8, the ligand RMSD values were all greater than 3.0 Å (Fig. S2). The results showed that the binding of the ligand molecules in the two structures M2 and M4 were more stable (Fig. 4b).

Finally, the composite structures M2 and M4 were subjected to eight 100 ns kinetic simulations (denoted D3 to D10, respectively), and the

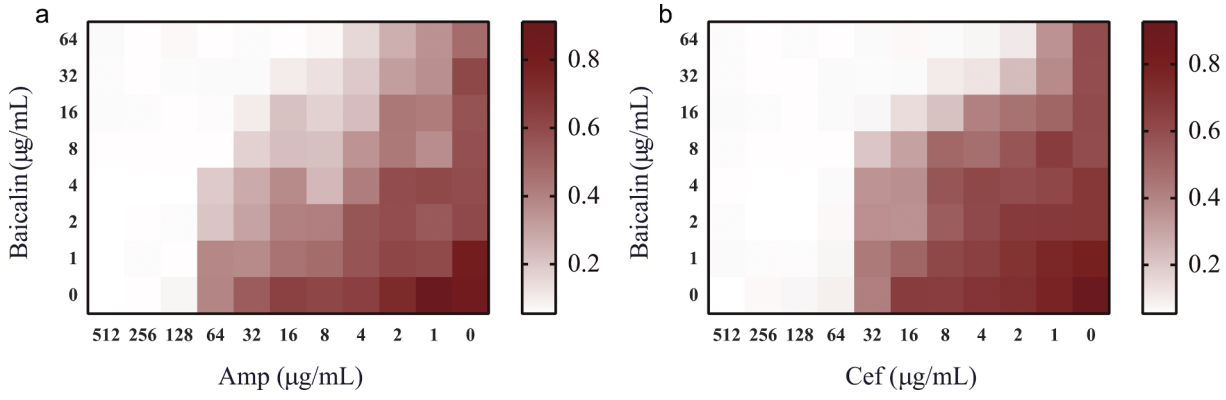

Fig. 2. Baicalin partially restores the susceptibility of *E.coli* BL21(DE3)/pET28a-NDM-1 to classical β-lactam antibiotics. (a, b) Microdilution checkerboard analysis showing the combined effect of Baicalin and classical β-lactam antibiotics against NDM-1 expressing *E. coli* BL21. Heat plots are the average of three replicates. At a concentration of 64 μg/ml, Baicalin reduces the MIC value for Ampcillin and Cefuroxime 16-fold, averagely.

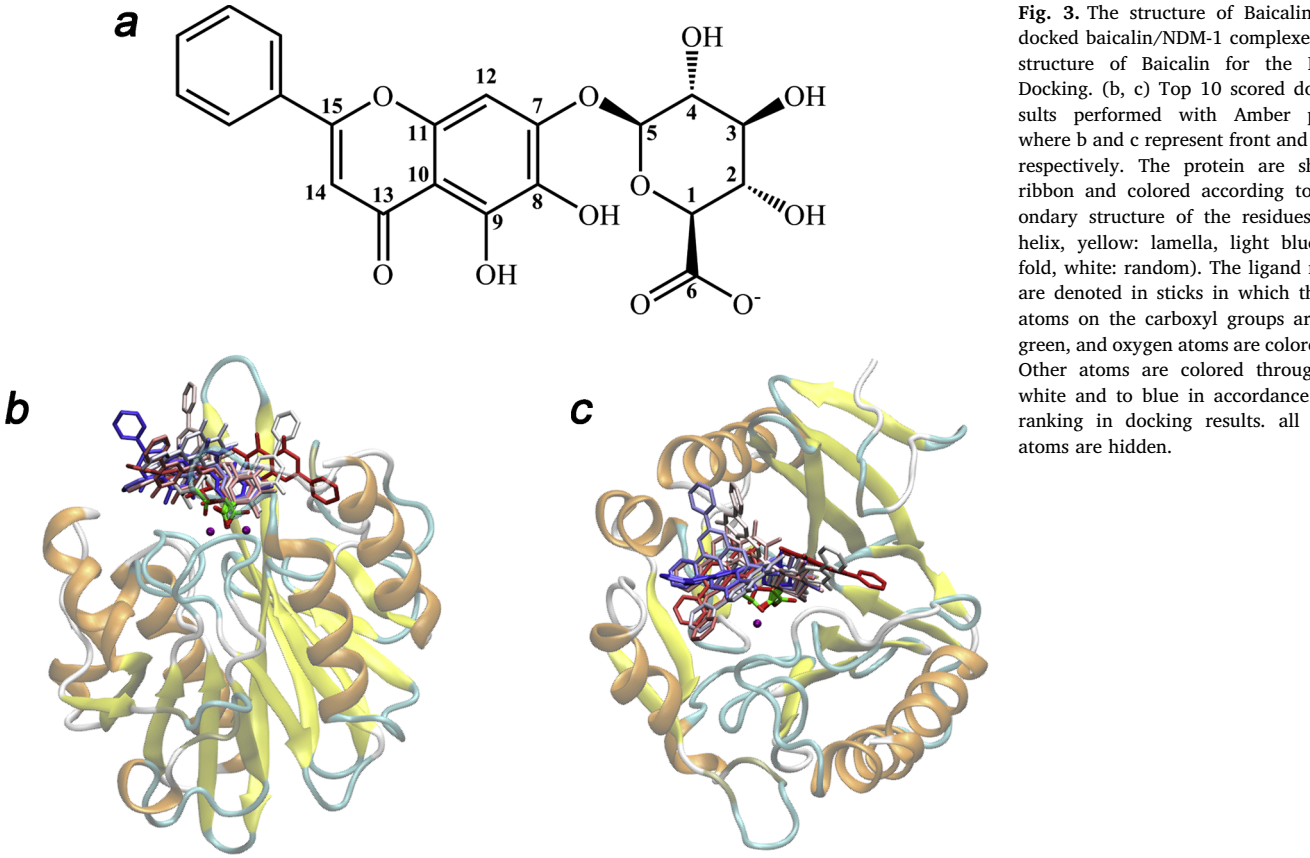

Fig. 3. The structure of Baicalin and the docked baicalin/NDM-1 complexes. (a) The structure of Baicalin for the Molecular Docking. (b, c) Top 10 scored docking results performed with Amber programs, where b and c represent front and top view, respectively. The protein are showed in ribbon and colored according to the secondary structure of the residues (orange: helix, yellow: lamella, light blue: double fold, white: random). The ligand molecules are denoted in sticks in which the carbon atoms on the carboxyl groups are colored green, and oxygen atoms are colored on red. Other atoms are colored through red to white and to blue in accordance with the ranking in docking results. all hydrogen atoms are hidden.

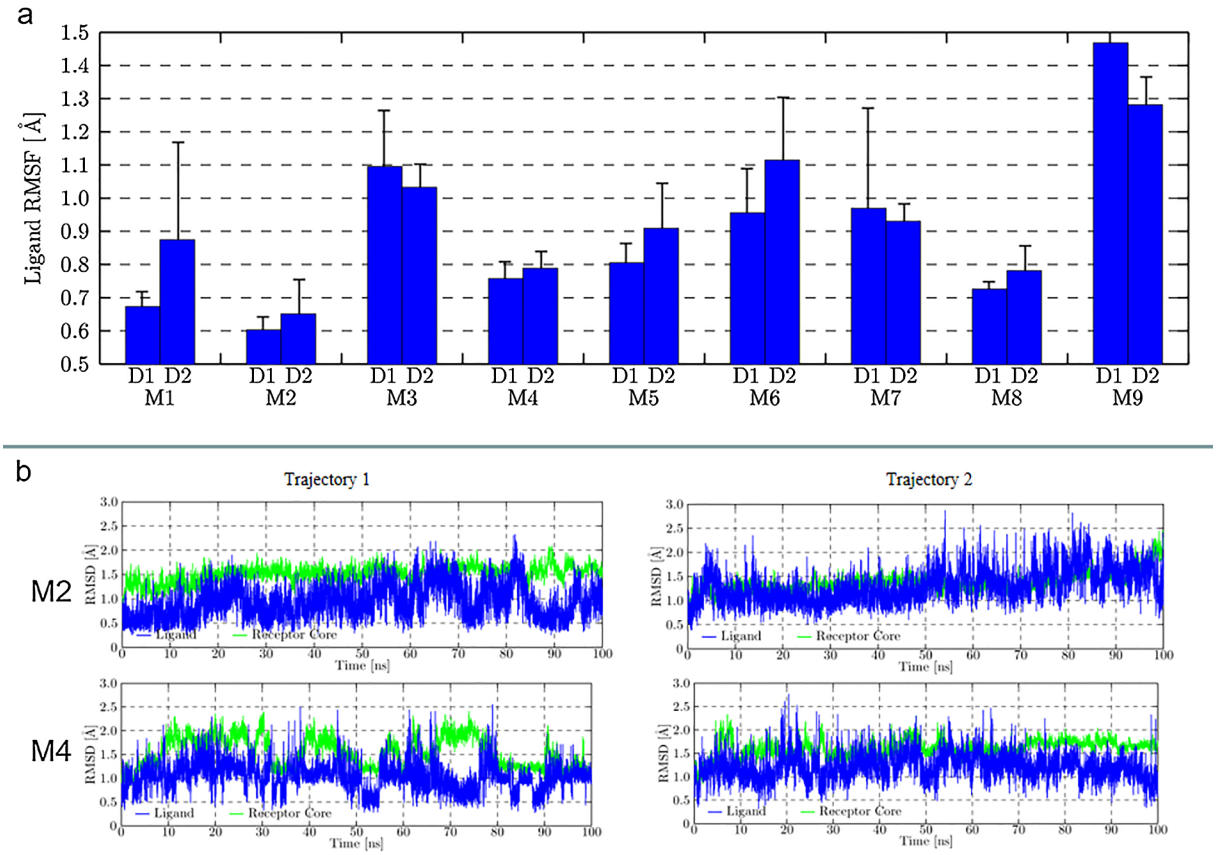

Fig. 4. a: Ligand RMSF value plot. D1 and D2 represent the two measured trajectories, respectively. The ordinate range is from 0.5 to 1.5 Å; b: The ligand (blue lines) and the pocket receptor residues (green lines) RMSDs of the M2 and M4. The vertical ranges from 0 to 3.0 Å.

Table 3
MMGBSA binding energy (unit: kcal/mol) of each trace of composite structure M2 and M4.

	M2	M4
D1	−9.72	−15.77
D2	−9.80	−15.73
D3	−10.47	−17.12
D4	−9.02	−10.35
D5	−8.87	−15.18
D6	−11.44	−13.54
D7	−10.89	−15.82
D8	−11.44	−14.93
D9	−10.36	−15.35
D10	−10.56	−9.94
Mean	−10.26	−14.37

MMGBSA binding energy between the complexes in these trajectories was calculated. The results obtained are shown in Table 3. The average MMGBSA binding energy of the composite structure M2 is −10.26 kcal/mol, and the average binding energy of the composite structure M4 is −14.37 kcal/mol. Since the binding energy of M4 is significantly more negative, The results showed that the binding ability between ligand and receptor in M4 is stronger than that of M2, so the complex structure M4 should be more reasonable.

3.4.2. Inter-complex interaction study

In order to explore the possible inhibition modes of Baicalin, the 10 trajectories of the relatively most reasonable complex structure M4 identified in 3.4.1 were clustered and the representative structure was obtained. At the same time, the MMGBSA binding energy between the complexes in each trajectory (except D4 and D10) was decomposed according to the residues, and then the contribution of each residue in the receptor (except for zinc ions and residues directly coordinating zinc ions) to ligand binding was observed, Receptor residues with an absolute energy contribution greater than 0.5 kcal/mol in the results of residue binding energy decomposition are reported in Table 4. It can be seen that the energy contribution value of a total of 5 residues is less than −0.5 kcal/mol, these residues should play a major role in promoting the binding of the ligand.

The structure of the complex obtained by clustering is shown in Fig. 5. It can be seen that the carboxyl group in the inhibitor Baicalin acts directly on the two zinc ions in the NDM-1 enzyme. The ligand C8 (the number of carbon atoms is shown in Fig. 3a) and the hydroxyl group on C9 will have a significant hydrogen bond with the carboxyl group of the side chain of Glu152, and the hydroxyl oxygen on C8 will also have a significant hydrogen bond with the backbone of Gln123. The hydrophobic side chains of the three residues Met67, Trp93 and Phe70 are located near the hydrophobic phenyl group of Baicalin. Combined with the energy contribution of Table 4, these residues may promote the binding of inhibitors through hydrophobic interaction. In addition, in the representative structure, the hydroxyl group on Baicalin C2 also forms hydrogen bonds with the side chain of Asn220 to promote the stability of the complex.

In summary, we speculate that the inhibitor molecule Baicalin is likely to directly bind to the zinc ion of the active center of the NDM-1 enzyme through its carboxyl group. At the same time, through the hydrogen bonding between Glu152, Gln123 and Asn220, and the hydrophobic interaction between Met67, Trp93 and Phe70, further stabled the binding of Baicalin.

Table 4
Receptor residues with MMGBSA binding energy contribution values less than −0.5 kcal/mol.

Residues	Energy contribution (kcal/mol)
Glu152	−3.008
Gln123	−2.437
Met67	−1.346
Trp93	−0.944
Phe70	−0.679

3.5. Discussion

In this study, Baicalin was identified as a potential NDM-1 inhibitor using virtual screen method. MIC experiments showed that it has the ability to restore the sensitivity of antibiotics to NDM-1, and its inhibition was confirmed by HPLC analysis. As an active ingredient of traditional Chinese medicine, Baicalin has been reported in synergistic effect with antibiotics and antivirals in recent years. For example, Zhao verified that baicalin has the ability to inhibit *E. coli* isolates in bovine mastoid milk and reduce antibiotic resistance [34]. Luo found that Baicalin can inhibit the formation of *P. aeruginosa* biofilm and enhance the bactericidal effect of various conventional antibiotics [35]. In addition, Wu has also identified its role in regulating bacterial virulence and host response as a promising agent for the prevention of *Salmonella typhimurium* infection [36]. These all show the broad prospects of Baicalin in the field of drug-resistant bacteria treatment. Considering the high safety of Baicalin itself, it can be used as a potential scaffold for future development of NDM-1 inhibitors.

Molecular dynamics can track the motion law of all particles at all times, and derive the simulation of the properties of the whole material, which is an effective means to study the microscopic world [37,38]. It has unique advantages in studying flexibility, cexploring the stability of composites and drug discovery [39,40]. In this study, Molecular dynamics explored the intrinsic interaction between Baicalin and NDM-1 complex and determined the relatively reasonable complex structure. It should be pointed out that the ligand stability in the first round of simulation can be maintained at the late stage of the trajectory, and the ligand stability of most complexes decreased significantly during the second round of molecular dynamics simulation. The reason for this may be that we recalculated the charge distribution on the atom based on the new ligand structure before the start of the second round of simulation. Since these new structures are significantly different from the original docking structure, the atomic charge on them may also change significantly. On the other hand, in the second round of simulation, the system re-experiences the energy optimization and temperature rise equilibrium process. All of these make the structure of the complex originally located in a certain energy valley, and in the new simulation it is likely that it is no longer in the same energy valley. At the same time, in the second round of calculation of RMSF value (Fig. 4), it can be seen that the RMSF values of the composites M1, M2, M4, M5 and M8 are small. However, considering that the ligand RMSD values in M1, M5, and M8 are more than 3.0 Å (Fig. S2), the binding of the ligand molecules in the two structures M2 and M4 is considered to be the most stable.

Finally, In inter-complex interaction study, We found that the carboxyl group in Baicalin directly interacts with the zinc ion in the active center of the enzyme, and the residues such as Glu152, Gln123, Met67, Trp93, and Phe70 in the enzyme further stabilize the binding of the inhibitor. From the above experimental results, it is speculated that the modification of the hydroxyl group at the C9 position of the Baicalin molecule to the amino group enhances the hydrophilic interaction with the Glu152 side chain, thereby enhancing the inhibitory activity of the inhibitor molecule, which needs further study.

4. Conclusion

Pathogenic bacteria expressing NDM-1 poses a real and escalating threat to human health. Although a number of compounds with great inhibitory activity have been reported, they still need to match some requirements including good synergistic effect with antibiotics, broad-spectrum inhibition, and reasonable pharmaceutical properties. There

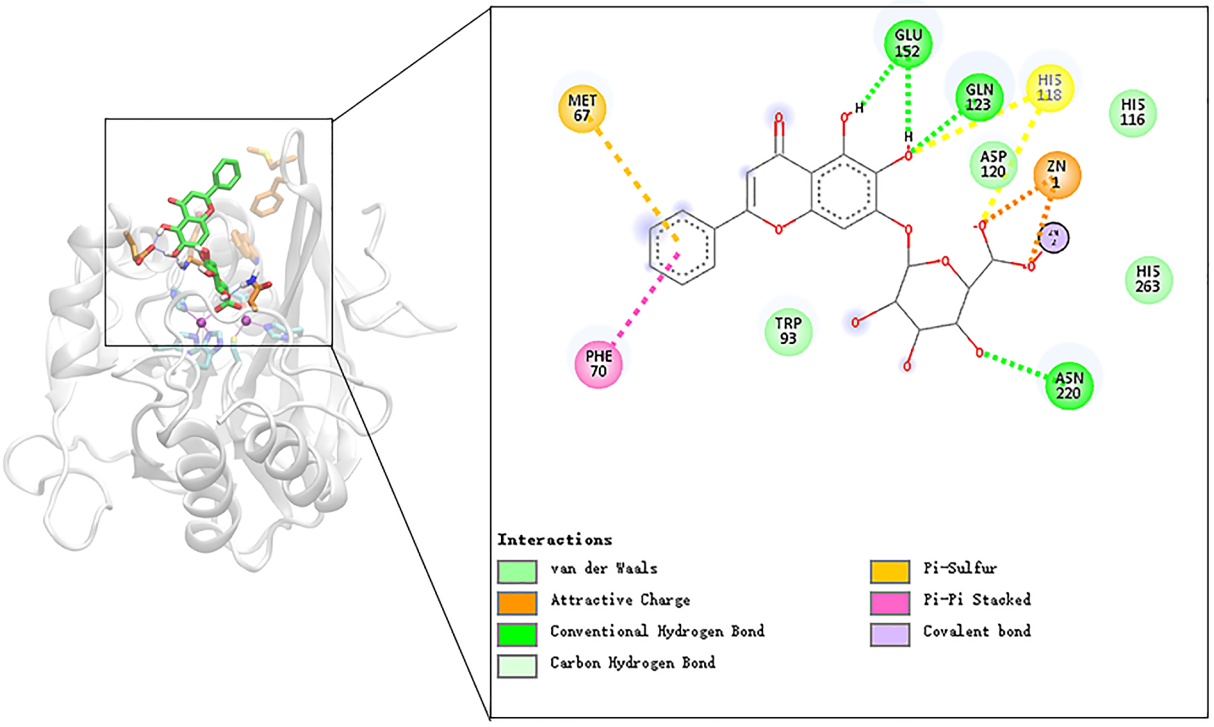

Fig. 5. Key interactions in representative structure of Baicalin/NDM-1 complex. The receptor is shown in a light gray ribbon. The two Zn^{2+} are purple balls and the oxygen atoms are red balls. Baicalin shows a green rod-like model that interacts with Zn^{2+} and key residues near the active center of the receptor.

is no doubt that the natural products perform an important function for drug development. Our group found an NDM-1 inhibitor Baicalin from a natural product library through virtual screening. *In vitro* experiments prove that Baicalin exhibits excellent inhibiting capacity on NDM-1 with IC_{50} 3.89 ± 1.1 μM, and efficiently restores the antibacterial activity of Ampcillin and Cefuroxime Sodium. Meanwhile, Molecular Docking and Dynamics simulations construct a rational complex structure of Baicalin and NDM-1 to explore the mechanism of inhibitory activity of Baicalin. Considered of the low toxicity character of Baicalin, it may serve as potential lead compound for anti-NDM-1 drug development.

Conflict of interest

The authors confirm that this article content has no conflicts of interest.

Acknowledgements

This work was supported by the National Natural Science Foundation of China (Grant Nos. 31300643 and 31370505), the Fundamental Research Funds for the Central Universities (Fund No. 2632018ZD04), the Priority Academic Program Development of Jiangsu Higher Education Institutions (PAPD) and Top-notch Academic Programs Project of Jiangsu Higher Education Institutions (TAPP). This research was also supported by High Performance Computing Center, China Pharmaceutical University, as well as Postgraduate Research & Practice Innovation Program of Jiangsu Province (Nos. SJKY19_0697 and SJCX18_0270). The funders had no role in study design, data collection and analysis, decision to publish, or preparation of the manuscript.

Appendix A. Supplementary material

Supplementary data to this article can be found online at https://doi.org/10.1016/j.bioorg.2019.102953.

References

[1] A. Versporten, G. Bolokhovets, L. Ghazaryan, et al., Antibiotic use in eastern Europe: a cross-national database study in coordination with the WHO Regional Office for Europe, Lancet Infect. Dis. 14 (5) (2014) 381–387, https://doi.org/10.1016/S1473-3099(14)70071-4.
[2] J.M. Blair, M.A. Webber, A.J. Baylay, et al., Molecular mechanisms of antibiotic resistance, Nat. Rev. Microbiol. 13 (1) (2015) 42–51, https://doi.org/10.1038/nrmicro3380.
[3] E.D. Brown, G.D. Wright, Antibacterial drug discovery in the resistance era, Nature 529 (7586) (2016) 336–343, https://doi.org/10.1038/nature17042.
[4] P. Ball, The clinical development and launch of amoxicillin/clavulanate for the treatment of a range of community-acquired infections, Int. J. Antimicrob. Ag. 30 (2007) S113–S117, https://doi.org/10.1016/j.ijantimicag.2007.07.037.
[5] G.D. Wright, Antibiotic adjuvants: rescuing antibiotics from resistance, Trends Microbiol. 24 (11) (2016) 862–871, https://doi.org/10.1016/j.tim.2016.06.009.
[6] M.T. Zmarlicka, M.D. Nailor, D.P. Nicolau, Impact of the New Delhi metallo-β-lactamase on β-lactam antibiotics, Infect. Drug Resist. 8 (2015) 297–309, https://doi.org/10.2147/IDR.S39186.
[7] A.P. Johnson, N. Woodford, Global spread of antibiotic resistance: the example of New Delhi metallo-beta-lactamase (NDM)-mediated carbapenem resistance, J. Med. Microbiol. 62 (Pt 4) (2013) 499–513, https://doi.org/10.1099/jmm.0.052555-0.
[8] P. Nordmann, L. Poirel, T.R. Walsh, D.M. Livermore, The emerging NDM carbapenemases, Trends Microbiol. 19 (2011) 588–595, https://doi.org/10.1016/j.tim.2011.09.005.
[9] R.J. Fair, Y. Tor, Antibiotics and bacterial resistance in the 21st century, Perspect. Med. Chem. 6 (2014) 25–64, https://doi.org/10.4137/PMC.S14459.
[10] R. Yuan, Y. Hou, W. Sun, et al., Natural products to prevent drug resistance in cancer chemotherapy: a review, Ann. N.Y. Acad. Sci. 1401 (1) (2017) 19–27, https://doi.org/10.1111/nyas.13387.
[11] N. Garg, T. Luzzatto-Knaan, A.V. Melnik, et al., Natural products as mediators of disease, Nat. Prod. Rep. 34 (2) (2017) 194–219, https://doi.org/10.1039/c6np00063k.
[12] A.M. King, S.A. Reid-Yu, W.L. Wang, et al., Aspergillomarasmine A overcomes metallo-beta-lactamase antibiotic resistance, Nature 510 (7506) (2014) 503–506, https://doi.org/10.1038/nature13445.
[13] S. Liu, Y. Zhou, X. Niu, et al., Magnolol restores the activity of meropenem against NDM-1-producing Escherichia coli by inhibiting the activity of metallo-beta-lactamase, Cell Death Discov. 4 (2018) 28, https://doi.org/10.1038/s41420-018-0029-6.
[14] J. Chiou, S. Wan, K.F. Chan, P.K. So, et al., Ebselen as a potent covalent inhibitor of New Delhi metallo-β-lactamase(NDM-1), Chem. Commun. (Camb) 51 (46) (2015) 9543–9546, https://doi.org/10.1039/c5cc02594j.
[15] C. Caddeo, A. Nacher, A. Vassallo, et al., Effect of quercetin and resveratrol co-incorporated in liposomes against inflammatory/oxidative response associated with skin cancer, Int. J. Pharm. 513 (1–2) (2016) 153–163.

[16] D. Benford, P.M. Bolger, P. Carthew, et al., Application of the Margin of Exposure (MOE) approach to substances in food that are genotoxic and carcinogenic, Food Chem. Toxicol. 48 (Suppl 1) (2010) S2–S24, https://doi.org/10.1016/j.fct.2009.09.024.
[17] M. Naïm, S. Bhat, K.N. Rankin, S. Dennis, Solvated interaction energy (SIE) for scoring protein-ligand binding affinities. 1. Exploring the parameter space, J. Chem. Inf. Model. 47 (1) (2007) 122–133, https://doi.org/10.1021/ci600406v.
[18] J. Chen, H. Chen, Y. Shi, et al., Probing the effect of the non-active-site mutation Y229W in New Delhi metallo-beta-lactamase-1 by site-directed mutagenesis, kinetic studies, and molecular dynamics simulations, PLoS One 8 (12) (2013) e82080, https://doi.org/10.1371/journal.pone.0082080.
[19] B. Shen, Y. Yu, H. Chen, et al., Inhibitor discovery of full-length New Delhi metallo-beta-lactamase-1 (NDM-1), PLoS One 8 (5) (2013) e62955, https://doi.org/10.1371/journal.pone.0062955.
[20] J.S. Kang, A.L. Zhang, M. Faheem, et al., Virtual screening and experimental testing of b1 metallo-β-lactamase inhibitors, J. Chem. Inf. Model. 58 (9) (2018) 1902–1914, https://doi.org/10.1021/acs.jcim.8b00133.
[21] J. Chen, H. Chen, T. Zhu, et al., Asp120Asn mutation impairs the catalytic activity of NDM-1 metallo-beta-lactamase: experimental and computational study, Phys. Chem. Chem. Phys. 16 (14) (2014) 6709–6716, https://doi.org/10.1039/c3cp55069a.
[22] J.D. Docquier, J. Lamotte-Brasseur, M. Galleni, et al., On functional and structural heterogeneity of VIM-type metallo-beta-lactamases, J. Antimicrob. Chemother. 51 (2) (2003) 257–266.
[23] F.C. Odds, Synergy, antagonism, and what the chequerboard puts between them, J. Antimicrob. Chemother. 52 (1) (2003) 1, https://doi.org/10.1093/jac/dkg301.
[24] Y.P. Pang, Successful molecular dynamics simulation of two zinc complexes bridged by a hydroxide in phosphotriesterase using the cationic dummy atom method, Proteins Struct. Funct. Bioinf. 45 (3) (2001) 183–189.
[25] W.L. Jorgensen, J. Chandrasekhar, J.D. Madura, et al., Comparison of simple potential functions for simulating liquid water, J. Chem. Phys. 79 (2) (1983) 926–935, https://doi.org/10.1371/journal.pone.0187292.
[26] P.F. Li, L.F. Song, K.M. Merz, Systematic parameterization of monovalent ions employing the nonbonded model, J. Chem. Theory Comput. (2015) 1645–1657, https://doi.org/10.1021/ct500918t.
[27] T. Darden, D. York, L. Pedersen, Particle mesh Ewald: an Nlog(N) method for Ewald sums in large systems, J. Chem. Phys. 98 (12) (1993) 10089–10092, https://doi.org/10.1002/jcc.21357.
[28] J.A. Izaguirre, D.P. Catarello, J.M. Wozniak, et al., Langevin stabilization of molecular dynamics, J. Chem. Phys. 114 (5) (2000) 2090–2098.
[29] J.P. Ryckaert, G. Ciccotti, H.J.C. Berendsen, Numerical integration of the cartesian equations of motion of a system with constraints: molecular dynamics of n-alkanes, J. Chem. Phys. 23 (3) (1977) 327–341.
[30] R. Faller, J.J.D. Pablo, Constant pressure hybrid molecular dynamics–Monte Carlo simulations, J. Chem. Phys. 116 (1) (2001) 55–59, https://doi.org/10.1007/s00894-014-2487-y.
[31] J. Ma, S. McLeod, K. MacCormack, et al., Real-time monitoring of New Delhi metallo-beta-lactamase activity in living bacterial cells by 1H NMR spectroscopy, Angew. Chem. Int. Ed. Engl. 53 (8) (2014) 2130–2133, https://doi.org/10.1039/c7cc02774e.
[32] X. Gao, M. Guo, Z. Zhang, et al., Baicalin promotes the bacteriostatic activity of lysozyme on S. aureus in mammary glands and neutrophilic granulocytes in mice, Oncotarget 8 (12) (2017) 19894–19901, https://doi.org/10.18632/oncotarget.15193.
[33] D.A. Case, T.E. Cheatham 3rd, T. Darden, et al., The Amber biomolecular simulation programs, J. Comput. Chem. 26 (16) (2005) 1668–1688.
[34] Q.Y. Zhao, F.W. Yuan, T. Liang, et al., Baicalin inhibits Escherichia coli isolates in bovine mastitic milk and reduces antimicrobial resistance, J. Dairy Sci. 101 (3) (2018) 2415–2422, https://doi.org/10.3168/jds.2017-13349.
[35] J. Luo, B. Dong, K. Wang, et al., Baicalin inhibits biofilm formation, attenuates the quorum sensing-controlled virulence and enhances Pseudomonas aeruginosa clearance in a mouse peritoneal implant infection model, PLoS One 12 (4) (2017) e0176883, , https://doi.org/10.1371/journal.pone.0176883.
[36] S.C. Wu, X.L. Chu, J.Q. Su, et al., Baicalin protects mice against Salmonella typhimurium infection via the modulation of both bacterial virulence and host response, Phytomedicine 48 (2018) 21–31, https://doi.org/10.1016/j.phymed.2018.04.063.
[37] Y1. Cai, J. Bao, X. Lao, et al., Computational design, functional analysis and antigenic epitope estimation of a novel hybrid of 12 peptides of hirudin and reteplase, J. Mol. Model. 21 (9) (2015) 229, https://doi.org/10.1007/s00894-015-2774-2.
[38] J. Yao, X. Qian, J. Bao, et al., Probing the effect of two heterozygous mutations in codon 723 of SLC26A4 on deafness phenotype based on molecular dynamics simulations, Sci. Rep. 5 (2015) 10831, https://doi.org/10.1038/srep10831.
[39] R. Suno, K.T. Kimura, T. Nakane, et al., Crystal structures of human orexin 2 receptor bound to the subtype-selective antagonist EMPA, Structure 26 (1) (2018) 7–19.e5, https://doi.org/10.1016/j.str.2017.11.005.
[40] X. Liu, D. Shi, S. Zhou, Molecular dynamics simulations and novel drug discovery, Exp. Opin. Drug Discov. 3 (1) (2018) 23–37, https://doi.org/10.1080/17460441.